Two-particle quantum walks: Entanglement and graph isomorphism testing

Scott D. Berry and Jingbo B. Wang*
School of Physics, University of Western Australia, 6009 Perth, Australia
(Received 17 February 2011; published 14 April 2011)

We study discrete-time quantum walks on the line and on general undirected graphs with two interacting or noninteracting particles. We introduce two simple interaction schemes and show that they both lead to a diverse range of probability distributions that depend on the correlations and relative phases between the initial coin states of the two particles. We investigate the characteristics of these quantum walks and the time evolution of the entanglement between the two particles from both separable and entangled initial states. We also test the capability of two-particle discrete-time quantum walks to distinguish nonisomorphic graphs. For strongly regular graphs, we show that noninteracting discrete-time quantum walks can distinguish some but not all nonisomorphic graphs with the same family parameters. By incorporating an interaction between the two particles, all nonisomorphic strongly regular graphs tested are successfully distinguished.

DOI: 10.1103/PhysRevA.83.042317 PACS number(s): 03.67.Ac, 03.65.Ud, 03.67.Bg, 02.10.Ox

I. INTRODUCTION

Single-particle quantum walks have recently emerged as a useful tool in the development of algorithms for quantum computers [1,2]. These algorithms depend on interference between the multiple paths that are simultaneously traversed by the quantum walker. In multiparticle quantum walks, the dimension of the state space increases exponentially with the number of particles and there is the additional possibility of entanglement between particles [3,4]. It is hoped that the greater complexity of the multiparticle walk may lead to more powerful applications, such as algorithms for the graph isomorphism problem [5,6]. There have also been some recent experimental realizations of two-particle quantum walks using both ions [7] and photons [8], demonstrating the technical feasibility of implementing quantum walks with more than one particle.

Like classical random walks, quantum walks come in both discrete-time and continuous-time variants. In this paper we focus on the discrete-time quantum walk. We mention the continuous-time case only in Sec. V when comparing the results of our quantum-walk-based graph isomorphism testing.

The theoretical study of discrete-time quantum walks with more than one particle was initiated by Omar *et al.* [3] who considered noninteracting two-particle quantum walks on the infinite line. Omar *et al.* established a role for entanglement in two-particle quantum walks by showing that initial states which are entangled in their coin degrees of freedom can generate two-particle probability distributions in which the positions of the two particles exhibit quantum correlations. Also with noninteracting particles, Štefaňák *et al.* [9] considered the meeting problem in the discrete-time quantum walk.

In addition to these studies with distinguishable particles, there have also been theoretical investigations of two-photon quantum walks [4,10]. By increasing the dimension of the coin Hilbert space to incorporate both the direction of photon propagation and polarization, Pathak and Agarwal [4] introduced a quantum walk in which two photons initially in separable Fock states become entangled through the action of linear optical elements. While the quantum walk studied in [3,9] requires entangled initial states to generate spatial correlations, the two-photon walk studied in [4], with its larger coin space, is capable of generating entanglement even from initially separable states. Venegas-Andraca and Bose [11] have also proposed a variant of the two-particle quantum walk in which the particles have a shared coin space. In this system, entanglement is introduced between the spatial degrees of freedom of the particles by performing measurements in the shared coin space.

In this work, we introduce spatial interactions between the particles and show that they generate entanglement between the two particles, even from initially separable states. We study the effect of correlations and relative phases between the initial coin states of the two particles on the time evolution of the quantum walks. For interacting walks, we find that these correlations and relative phases provide an additional resource for tuning the time evolution of the quantum walk that is not accessible in noninteracting two-particle quantum walks.

The interaction schemes considered here preserve the unitary nature of the quantum walk and can be applied to two-particle quantum walks on arbitrary graphs, with higher than two-dimensional coin spaces. This allows us to numerically test the capability of interacting and noninteracting quantum walks to distinguish nonisomorphic strongly regular graphs.

The paper is structured as follows. In Sec. II we describe the mathematical formalism for noninteracting and interacting two-particle quantum walks. Results for the single- and two-particle probability distributions obtained for these quantum walks are presented in Sec. III and in Sec. IV we present numerical calculations of the time evolution of entanglement between the particles. In Sec. V, we discuss an application to graph isomorphism testing. Finally, Sec. VI contains our conclusions.

II. QUANTUM WALKS

A. Review of single-particle quantum walks

1. Quantum walk on the line

We begin by briefly reviewing the single-particle quantum walk on the infinite line. Each position on the line is associated

*wang@physics.uwa.edu.au

with a two-dimensional auxiliary "coin" Hilbert space $\mathcal{H}_C$, spanned by the orthonormal basis $\{|\uparrow\rangle,|\downarrow\rangle\}$. The quantum walk on the line then takes place in the product space $\mathcal{H}_P \otimes \mathcal{H}_C$, where $\mathcal{H}_P$ is the position Hilbert space with orthonormal basis given by the position states $\{|x\rangle, x \in \mathbb{Z}\}$. One step of the walk is defined as a single application of the unitary time-evolution operator $U = S(\mathbb{1} \otimes C)$. The shifting operator S is defined as

$$S := |x+1, \uparrow\rangle\langle x, \uparrow| + |x-1, \downarrow\rangle\langle x, \downarrow|. \tag{1}$$

For each position x, the coin operator C can be represented by a 2×2 unitary matrix which acts on $\mathcal{H}_C$ as

$$C\begin{pmatrix} a_\uparrow \\ a_\downarrow \end{pmatrix} = \begin{pmatrix} \sqrt{\rho} & \sqrt{1-\rho}\, e^{i\theta} \\ \sqrt{1-\rho}\, e^{i\phi} & -\sqrt{\rho}\, e^{i(\theta+\phi)} \end{pmatrix}\begin{pmatrix} a_\uparrow \\ a_\downarrow \end{pmatrix}, \tag{2}$$

where $a_\uparrow = \langle x, \uparrow|\psi\rangle$ and $a_\downarrow = \langle x, \downarrow|\psi\rangle$ are the probability amplitudes for the $|\uparrow\rangle$ and $|\downarrow\rangle$ coin states, respectively. Setting $\rho = 1/2$ and $\theta = \phi = 0$ gives the standard Hadamard coin. Since the action of the shifting operator depends on the coin state of the particle, the shifting operator entangles the coin and position of the particle throughout the quantum walk [12].

2. *Quantum walks on graphs*

The quantum walk on the line described above can be extended to a general undirected graph [13]. Let $G(V,E)$ be an undirected graph with vertex set $V = \{v_1, v_2, v_3, \ldots\}$ and edge set $E = \{(v_i,v_j),(v_k,v_l), \ldots\}$ consisting of unordered pairs of connected vertices. If there are d edges incident on a vertex v_i, we say that v_i has degree d. In this case $\mathcal{H}_P$ is spanned by an orthonormal basis of vertex states $\{|v_i\rangle : v_i \in V\}$ and $\mathcal{H}_C$ is spanned by an orthonormal basis of coin states $\{|c_i\rangle : i = 1, \ldots, d\}$, representing the outgoing edges at a vertex v_i. The discrete-time quantum walk on a graph takes place on the subnodes of the graph, which are represented by product states of the form $|v\rangle \otimes |c\rangle = |v,c\rangle \in \mathcal{H}_P \otimes \mathcal{H}_C$.

S is redefined in this basis to shift the probability amplitudes between connected subnodes,

$$S|v_i,c_j\rangle = |v_j,c_i\rangle, \tag{3}$$

where $|v_i,c_j\rangle$ is the subnode state corresponding to the edge (v_i,v_j) at the vertex v_i. The coin operator C at a vertex v_i of degree d_i can be represented by a $d_i \times d_i$ matrix which mixes the probability amplitudes of the subnode states of v_i. The only coin operator considered in this paper for quantum walks on graphs is the Grover coin G,

$$G_{ij} = -\delta_{ij} + 2/d, \tag{4}$$

for a vertex of degree $d > 2$.

B. Noninteracting two-particle quantum walks

1. *Two-particle quantum walk on the line*

A two-particle quantum walk takes place in the Hilbert space $\mathcal{H} = \mathcal{H}_1 \otimes \mathcal{H}_2$, where $\mathcal{H}_i = (\mathcal{H}_P \otimes \mathcal{H}_C)_i$ for particle i, as described in [3]. Let

$$|x,\alpha\,;y,\beta\rangle := |x,\alpha\rangle_1 \otimes |y,\beta\rangle_2 \tag{5}$$

be a two-particle basis state, where x,y represent the positions of particles 1 and 2 and $\alpha,\beta \in \{\uparrow, \downarrow\}$ represent their respective coin states. The time-evolution operator is defined as

$$U := S(\mathbb{1} \otimes C), \tag{6}$$

where S is defined in the two-particle basis by

$$\begin{aligned} S := {} & |x+1, \uparrow\,; y+1, \uparrow\rangle\langle x, \uparrow\,; y, \uparrow| \\ & + |x+1, \uparrow\,; y-1, \downarrow\rangle\langle x, \uparrow\,; y, \downarrow| \\ & + |x-1, \downarrow\,; y+1, \uparrow\rangle\langle x, \downarrow\,; y, \uparrow| \\ & + |x-1, \downarrow\,; y-1, \downarrow\rangle\langle x, \downarrow\,; y, \downarrow|. \end{aligned} \tag{7}$$

For a particular x and y, the coin operator can be represented as a 4×4 matrix $C = C_1 \otimes C_2$. For example, if C_1 and C_2 are both equal to the standard 2×2 Hadamard matrix then C acts on the coin Hilbert space as

$$C\begin{pmatrix} a_{\uparrow\uparrow} \\ a_{\downarrow\uparrow} \\ a_{\uparrow\downarrow} \\ a_{\downarrow\downarrow} \end{pmatrix} = \frac{1}{2}\begin{pmatrix} 1 & 1 & 1 & 1 \\ 1 & -1 & 1 & -1 \\ 1 & 1 & -1 & -1 \\ 1 & -1 & -1 & 1 \end{pmatrix}\begin{pmatrix} a_{\uparrow\uparrow} \\ a_{\downarrow\uparrow} \\ a_{\uparrow\downarrow} \\ a_{\downarrow\downarrow} \end{pmatrix}, \tag{8}$$

where $a_{\alpha\beta} := \langle x,\alpha\,;y,\beta|\psi\rangle$. For noninteracting walks, C is taken to be identical for all two-particle position states.

In order to study the two-particle quantum walk, it is necessary to consider not only the single-particle probability distributions of each of the two particles, but also the relationship between these distributions. The *two-particle probability distribution*, $P(x,y,t)$, is the probability of finding particle 1 at position x and particle 2 at position y after t steps of the two-particle quantum walk, i.e.,

$$P(x,y,t) = \sum_{\alpha,\beta=\uparrow,\downarrow} |\langle x,\alpha\,;y,\beta|(U)^t|\psi_0\rangle|^2, \tag{9}$$

where $|\psi_0\rangle$ is the initial state of the system.

2. *Two-particle quantum walks on graphs*

By analogy with single-particle quantum walks on graphs described in Sec. II A 2, we can extend the formalism introduced for two-particle walks on the line to general undirected graphs. The two-particle basis for the Hilbert space $\mathcal{H}$ now consists of states of the form $|v_i,c_j\,;v_k,c_l\rangle := |v_i,c_j\rangle_1 \otimes |v_k,c_l\rangle_2$. The time-evolution operator U is defined as $U = S(\mathbb{1} \otimes C)$, where S is the two-particle shift operator and C is the two-particle coin operator. $S = S_1 \otimes S_2$ acts on a two-particle basis state as

$$S|v_i,c_j\,;v_k,c_l\rangle = |v_j,c_i\,;v_l,c_k\rangle. \tag{10}$$

The coin operator C_{ik} can be represented as a $d_i d_k \times d_i d_k$ matrix given by $(C_1)_i \otimes (C_2)_k$, where $(C_1)_i$ is the $d_i \times d_i$ coin matrix for the vertex state $|v_i\rangle_1$ and $(C_2)_k$ is the $d_k \times d_k$ coin matrix for the vertex state $|v_k\rangle_2$. The matrix C_{ik} acts on the $d_i d_k$-dimensional two-particle coin state basis with the following ordering of basis states, $\{|c_1,c_1\rangle,|c_2,c_1\rangle, \ldots,|c_{d_i},c_1\rangle, |c_1,c_2\rangle,|c_2,c_2\rangle, \ldots,|c_{d_i-1},c_{d_k}\rangle,|c_{d_i},c_{d_k}\rangle\}$.

C. Interacting two-particle quantum walks

For the noninteracting quantum walks considered above, the single-particle probability distributions for each particle

evolve independently. We now consider incorporating an explicit interaction between the particles. We introduce two alternative interaction schemes, which will be referred to as the $\mathbb{1}$ interaction and the π-phase interaction. These interactions have not previously been considered.

For two-particle quantum walks on both the line and on graphs, the $\mathbb{1}$ interaction is implemented by substituting the standard coin operator with the negative identity operator when both of the particles are in the same position (or vertex) state. For example, in the two-particle quantum walk on the line with the Hadamard coin H, the coin operator for the states $\{|x,\alpha;y,\beta\rangle,\alpha,\beta \in \{\uparrow,\downarrow\}\}$ becomes

$$C = \begin{cases} H \otimes H & \text{when} \quad x \neq y, \\ -\mathbb{1} \otimes -\mathbb{1} = \mathbb{1} & \text{when} \quad x = y. \end{cases} \tag{11}$$

This interaction is introduced by analogy with the quantum-walk-based search procedure described in [14], in which a quantum oracle is implemented as a substitution of the Grover coin operator at the "marked" vertices. In some sense, the $\mathbb{1}$-interacting two-particle walk is equivalent to the search procedure with all doubly occupied vertex states being "marked."

The π-phase interaction is similar to the above $\mathbb{1}$ interaction; however, when both particles are at the same vertex, rather than using the identity coin operator, we shift the phase of all subnode states by π. For example, in the two-particle quantum walk on the line with the Hadamard coin H, the π-phase interacting quantum walk coin operator becomes

$$C = \begin{cases} H \otimes H & \text{when} \quad x \neq y, \\ e^{i\pi} H \otimes H & \text{when} \quad x = y. \end{cases} \tag{12}$$

Neither of these interactions are intended to represent particular physical situations. We study them here as they allow us to examine characteristics of the two-particle quantum walks that are affected by explicit spatial interactions between particles.

III. PROBABILITY DISTRIBUTIONS

It is well known that for a single-particle quantum walk on the infinite line with the Hadamard coin, the unbiased initial state $|\psi_0\rangle = \frac{1}{\sqrt{2}}(|0,\uparrow\rangle_1 + i|0,\downarrow\rangle_1)$ generates a probability distribution that is symmetric about the origin [15]. For two-particle quantum walks, we consider a separable product state formed from two particles, each in this unbiased state,

$$\begin{aligned} |\text{sep}\rangle &= \tfrac{1}{2}(|0,\uparrow\rangle_1 + i|0,\downarrow\rangle_1) \otimes (|0,\uparrow\rangle_2 + i|0,\downarrow\rangle_2) \\ &= \tfrac{1}{2}(|0,\uparrow;0,\uparrow\rangle + i|0,\uparrow;0,\downarrow\rangle \\ &\quad + i|0,\downarrow;0,\uparrow\rangle - |0,\downarrow;0,\downarrow\rangle). \end{aligned} \tag{13}$$

We also consider the Bell states $|\Psi^+\rangle, |\Psi^-\rangle, |\Phi^+\rangle$, and $|\Phi^-\rangle$ in which the coin states of the two particles are maximally entangled:

$$|\Psi^+\rangle = \frac{1}{\sqrt{2}}(|0,\uparrow;0,\downarrow\rangle + |0,\downarrow;0,\uparrow\rangle), \tag{14}$$

$$|\Psi^-\rangle = \frac{1}{\sqrt{2}}(|0,\uparrow;0,\downarrow\rangle - |0,\downarrow;0,\uparrow\rangle), \tag{15}$$

$$|\Phi^+\rangle = \frac{1}{\sqrt{2}}(|0,\uparrow;0,\uparrow\rangle + |0,\downarrow;0,\downarrow\rangle), \tag{16}$$

$$|\Phi^-\rangle = \frac{1}{\sqrt{2}}(|0,\uparrow;0,\uparrow\rangle - |0,\downarrow;0,\downarrow\rangle). \tag{17}$$

Note that for all initial states considered here ($|\text{sep}\rangle, |\Psi^\pm\rangle, |\Phi^\pm\rangle$), the probability of measuring particle i in the $|\uparrow\rangle$ or $|\downarrow\rangle$ coin state is equal to $1/2$, for $i = 1,2$.

The two-particle probability distribution obtained for a Hadamard walk on the line using the initial separable state $|\text{sep}\rangle$ is simply the product of two standard Hadamard single-particle probability distributions [3]. That is, for the noninteracting two-particle quantum walk, when there is no entanglement between the particles in the initial state, both quantum walks evolve independently and no correlations are introduced between the positions of the particles.

The entangled initial states $|\Psi^+\rangle$ and $|\Psi^-\rangle$ were also studied in [3]. It was found that while the single-particle probability distributions obtained from both initial states were identical, the two-particle probability distributions revealed correlations between the positions of the particles at later times that depend on the relative phases between the coin states of the two particles. We find similar results for the initial states $|\Phi^+\rangle$ and $|\Phi^-\rangle$.

We now consider the interacting two-particle quantum walks described in Sec. II C. The results of incorporating the $\mathbb{1}$ interaction and the π-phase interaction on the time evolution of the two-particle quantum walk are shown in Figs. 1 and 2, respectively. In the noninteracting walk, the single-particle probability distributions are independent of whether or not the coins of the two particles are entangled in the initial state. It can be seen, however, that for the interacting quantum walks, different correlations and relative phases between the initial coin states of the two particles generate different single-particle probability distributions. This arises because the interacting quantum walk depends on the relative positions of the two particles, which in turn depends on the correlations and relative phases between the initial coin states of the two particles.

First, we examine the results for the $\mathbb{1}$ interaction in more detail. In Fig. 1(a), the time evolution of the quantum walk from the initial separable state $|\text{sep}\rangle$ is shown. This initial state results in part of the probability distribution traveling linearly outward from the origin without spreading. This is caused by the $|0,\uparrow;0,\uparrow\rangle$ and $|0,\downarrow;0,\downarrow\rangle$ terms in $|\text{sep}\rangle$. In the interacting walk the $\mathbb{1}$ coin operator acts on these states because both particles are at the same position. Since both particles are also in the same coin state and the $\mathbb{1}$ operator does not mix the coin states of each particle, they are translated together and move in the same direction at each step of the walk. This is also observed in Figs. 1(g) and 1(i) for the initial states $|\Phi^+\rangle$ and $|\Phi^-\rangle$.

The remaining terms in $|\text{sep}\rangle$ that are not immediately separated by the $\mathbb{1}$ interaction are equivalent to the entangled state $|\Psi^+\rangle$ and result in a similar probability distribution [Fig. 1(c)]. As shown in Fig. 1(c), the single-particle probability distribution for the state $|\Psi^+\rangle$ is identical to that obtained for the noninteracting walk with the same initial state. The initial entangled state $|\Psi^-\rangle$ results in the unusual single-particle probability distribution shown in Fig. 1(e). The $\mathbb{1}$ interaction in this case results in two peaks moving in either

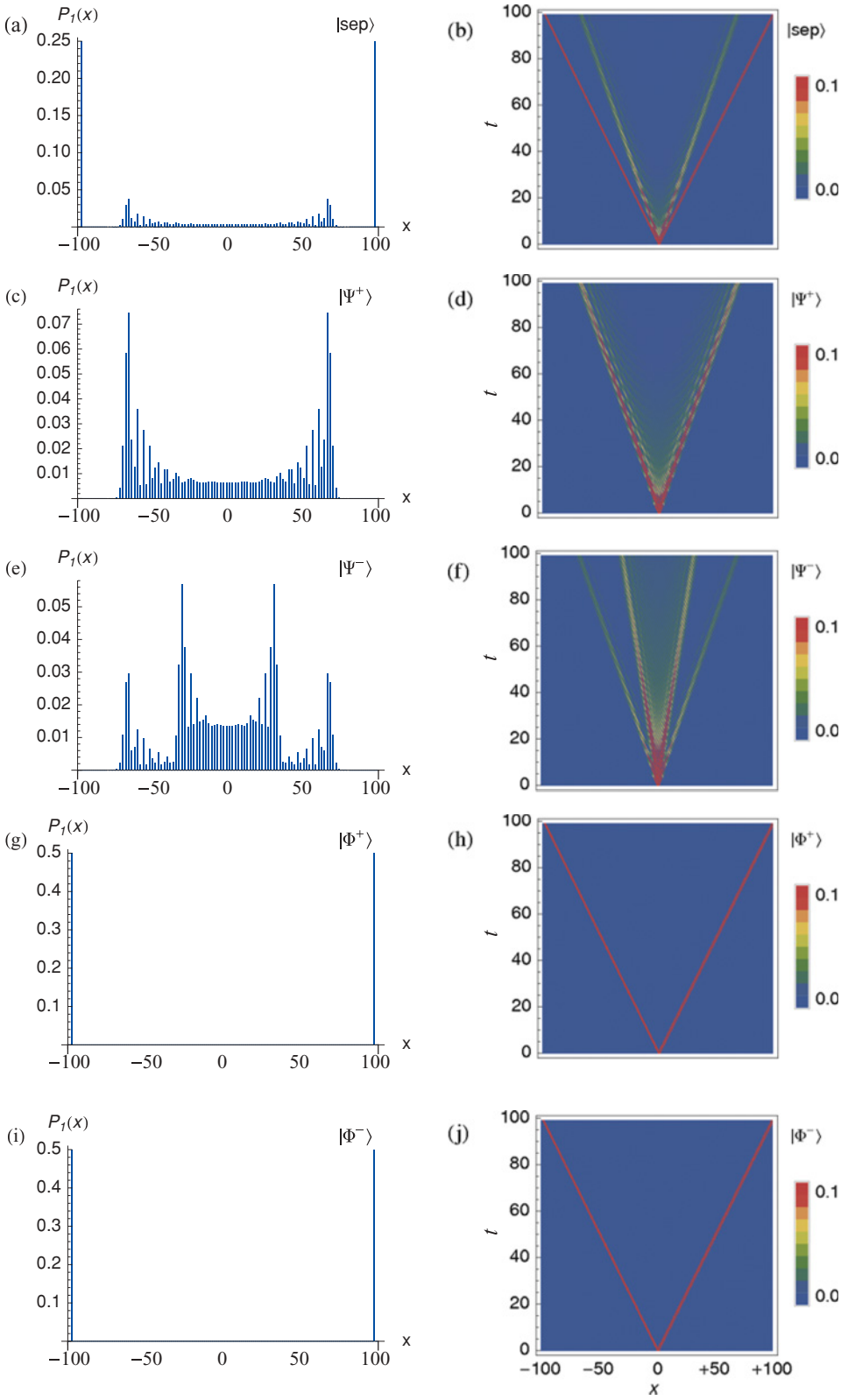

FIG. 1. (Color online) Single-particle probability distributions after 100 steps of an $\mathbb{1}$-interacting Hadamard walk on the infinite line, for the initial states shown. Also shown is the time evolution of the probability distribution from the initially localized state.

direction. The fastest moving peak spreads with the usual speed and the slower of the peaks spreads with approximately half the speed. The interaction results in a slowing of the propagation of the walk for the portion of the probability distribution which does not immediately escape the local spatial interaction.

Next we consider the π-phase interaction. From Fig. 2, it can be seen that the diversity of single-particle probability distributions obtained with the π-phase interaction is much greater than with the $\mathbb{1}$ interaction. The behavior seen for $|\text{sep}\rangle$, $|\Phi^+\rangle$, and $|\Phi^-\rangle$ in the $\mathbb{1}$-interacting walk no longer occurs in the π-phase interacting walk because the Hadamard coin is

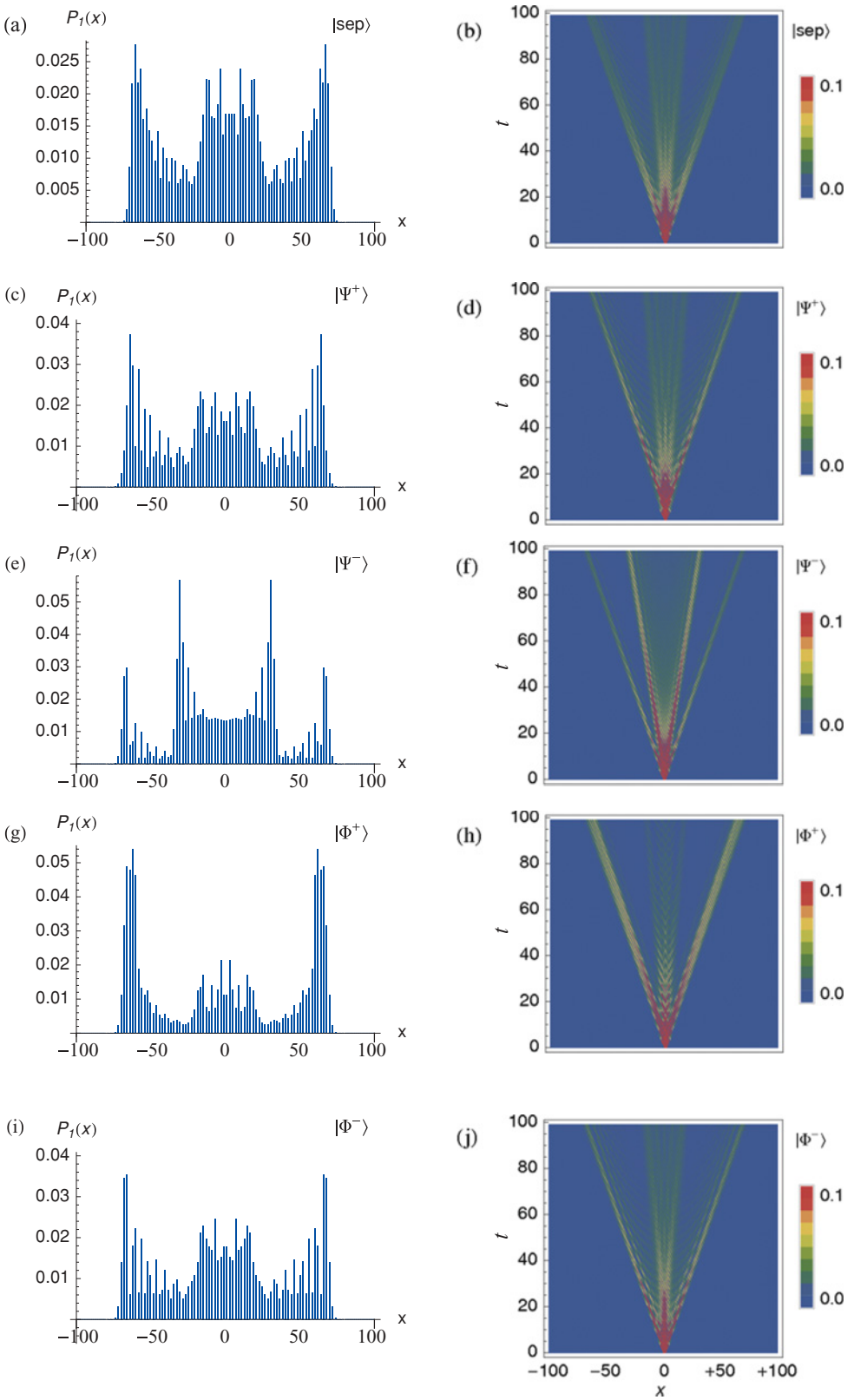

FIG. 2. (Color online) Single-particle probability distributions after 100 steps of a π-phase interacting Hadamard walk on the infinite line, for the initial states shown. Also shown is the time evolution of the probability distribution from the initially localized state.

applied to all position states at each step of the walk, mixing the coin states at each position. It should be noted that none of the single-particle probability distributions obtained are similar to the noninteracting two-particle quantum walk and also that the single-particle probability distributions obtained for both interaction schemes are identical for the initial state $|\Psi^-\rangle$ [Figs. 1(e) and 2(e)].

Figures 3 and 4 compare the two-particle probability distributions obtained from quantum walks with the $\mathbb{1}$ interaction and with the π-phase interaction for the same initial

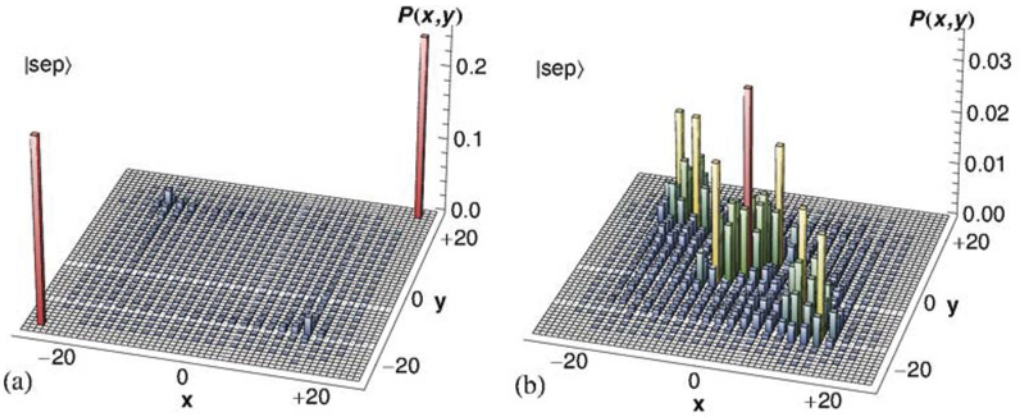

FIG. 3. (Color online) Two-particle probability distributions after 25 steps of a two-particle quantum walk on the infinite line for (a) the $\mathbb{1}$ interaction and (b) the π-phase interaction, from the separable initial state $|\text{sep}\rangle$.

states. It can be seen that the interactions generate spatial correlations between the two particles for all initial states. This is notably different behavior from the noninteracting quantum walk, where initial coin space entanglement between the two particles is required to generate spatial correlations [3].

As can be seen in Figs. 3 and 4, the peaks which are farthest from the origin of the walk are anticorrelated in position for all initial states. This means that if, upon measurement of the system, one particle is found to be relatively far from the origin of the walk then the other particle is likely to be found at the opposite end of the line. These interacting quantum walks may therefore be useful for generating spatially correlated pairs of particles from arbitrary localized initial states. In addition, for all initial states considered, the π-phase interaction generates probability distributions in which both particles have a high probability of bunching together, close to the origin of the walk.

We have shown that these interactions introduce spatial correlations between the two particles. We therefore find it interesting to quantify the entanglement generated between the particles in these quantum walks.

IV. ENTANGLEMENT BETWEEN PARTICLES

Entanglement between the coin and position in single-particle quantum walks on regular graphs has been well studied [12,16–18]. There has also been a study of the entanglement between lattice positions in single- and (noninteracting) many-particle quantum walks on the infinite line [19]; however, this does not quantify the entanglement between the positions of the particles undergoing the quantum walk.

We use the von Neumann entropy to measure the total entanglement between the subsystems describing each of the two particles in quantum walks on arbitrary graphs.

The entanglement between two subsystems of a bipartite pure quantum state $|\psi\rangle$ can be quantified using the von Neumann entropy S of the reduced density matrix of either subsystem [20],

$$E(|\psi\rangle) = S(\rho_1) = S(\rho_2) = -\text{Tr}(\rho_1 \log_2 \rho_1), \tag{18}$$

with $\mathbf{0}\log_2 \mathbf{0} := \mathbf{0}$. Since the trace is invariant under similarity transformation and the density matrix ρ_1 has real, nonnegative eigenvalues λ_i, the von Neumann entropy is most easily calculated as

$$S(\rho_1) = -\sum_i \lambda_i \log_2 \lambda_i. \tag{19}$$

For two-particle quantum walks, the composite space $\mathcal{H}$ can be partitioned into single-particle subsystems, $\mathcal{H}_{1(2)} = (\mathcal{H}_\mathcal{P} \otimes \mathcal{H}_\mathcal{C})_{1(2)}$, to give a measure of the total entanglement between the two particles.

In the following, x,y,z,w represent vertices in a graph, while i,j,k,l represent coin states and $a_{xiyj} \in \mathbb{C}$ are coefficients of the two-particle basis states. For the pure state $|\psi\rangle \in \mathcal{H}$,

$$|\psi\rangle = \sum_{xy}\sum_{ij} a_{xiyj}|x,i\,;y,j\rangle, \tag{20}$$

the reduced density matrix ρ_1 is obtained by tracing the density matrix $\rho = |\psi\rangle\langle\psi|$ over subsystem 2,

$$\rho_1 = \text{Tr}_2(\rho) = \sum_{xyzw}\sum_{ijkl} a_{xiyj}a^*_{zkwl}|x,i\rangle\langle z,k|\langle w,l|y,j\rangle. \tag{21}$$

Using the orthonormality of the subnode states $\langle w,l|y,j\rangle = \delta_{yw}\delta_{jl}$, we obtain

$$\rho_1 = \sum_{xz}\sum_{ik} b_{xizk}|x,i\rangle\langle z,k|, \tag{22}$$

where $b_{xizk} = \sum_y \sum_j a_{xiyj}a^*_{zkyj}$.

Equation (22) provides a direct method for calculating ρ_1 from the coefficients a_{xiyj}. Numerical methods can then be used to calculate the eigenvalues of ρ_1, and from Eqs. (18) and (19), the entanglement E between the two particles can be obtained at each time step.

The maximum value of entanglement E between two k-dimensional subsystems is $E_{\max} = \log_2 k$. In the quantum walk on the infinite line, the coin space is two dimensional. If both particles are initially localized at the origin, then the position space is one dimensional, so the Bell states $|\Psi^\pm\rangle, |\Phi^\pm\rangle$ are maximally entangled ($E_{\max} = \log_2 2 = 1$). As the quantum walk can spread at a rate of one lattice position per time step in each direction, the number of possible occupied states in a two-particle quantum walk on the infinite line increases linearly

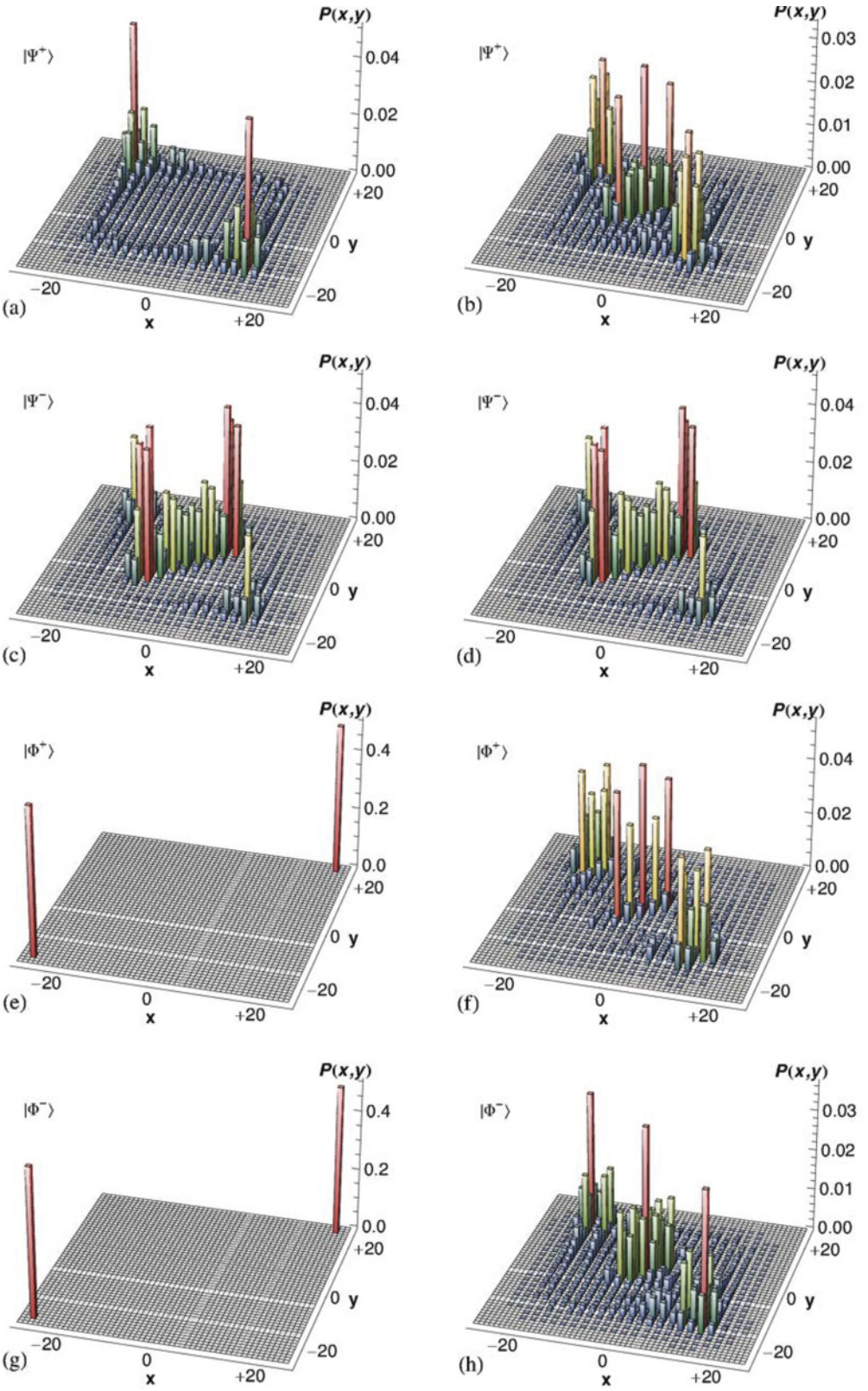

FIG. 4. (Color online) Two-particle probability distributions after 25 steps of a two-particle quantum walk on the infinite line for (left panel) the $\mathbb{1}$ interaction and (right panel) the π-phase interaction, from initial states shown.

with the number of steps. The dimension of each of the single-particle subspaces is therefore $k = 2(2t + 1)$, giving $E_{\max} = \log_2[2(2t + 1)] = 1 + \log_2(2t + 1)$. So the upper bound on entanglement grows logarithmically with the number of steps in the walk. For an N-cycle, the subsystems of the individual particles each have dimension $k = 2N$, so the upper bound on

entanglement is fixed at $E_{\max} = \log_2 2N$. For the 16-cycle, a maximally entangled bipartite state has $E = \log_2 32 = 5$.

Numerical evaluation of the entanglement between the particles in noninteracting two-particle quantum walks demonstrates that the entanglement between the particles does not change throughout the evolution of the walk, $E(|\text{sep}\rangle) \equiv 0$ and $E(|\psi\rangle) \equiv 1$ for $\psi \in \{\Psi^{\pm}, \Phi^{\pm}\}$, for all $t \geqslant 0$. This is consistent with the fact that each of the single-particle probability distributions evolve independently in this case.

For the interacting cases, the spatial correlations observed between the particles in Fig. 3 suggest that the interactions can generate entanglement between the two particles even from initially separable states. Numerical evaluation of the time evolution of entanglement between the particles in interacting quantum walks on the infinite line and 16-cycle are shown in Figs. 5 and 6, respectively, for initial states $|\text{sep}\rangle, |\Psi^{\pm}\rangle$, and $|\Phi^{\pm}\rangle$. It can be seen that both interactions are capable of generating entanglement between the particles.

It is also apparent that for both the infinite line and the 16-cycle, the entanglement introduced by the π-phase interaction is generally greater than the entanglement generated from the same initial state by the $\mathbb{1}$ interaction. The Bell states $|\Phi^{\pm}\rangle$, which propagate linearly outward without mixing in the $\mathbb{1}$-interacting quantum walk, maintain a constant entanglement, $E = 1$, while for the same initial states, the π-phase interaction

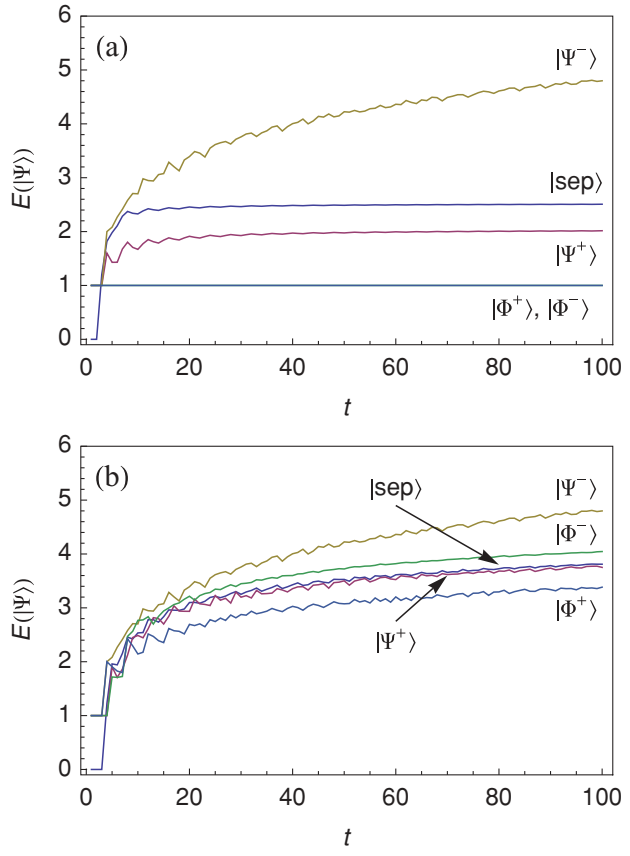

FIG. 5. (Color online) Time evolution of the entanglement between the two particles for (a) the $\mathbb{1}$-interacting and (b) the π-phase interacting quantum walk on the infinite line using the Hadamard coin, from initial states shown.

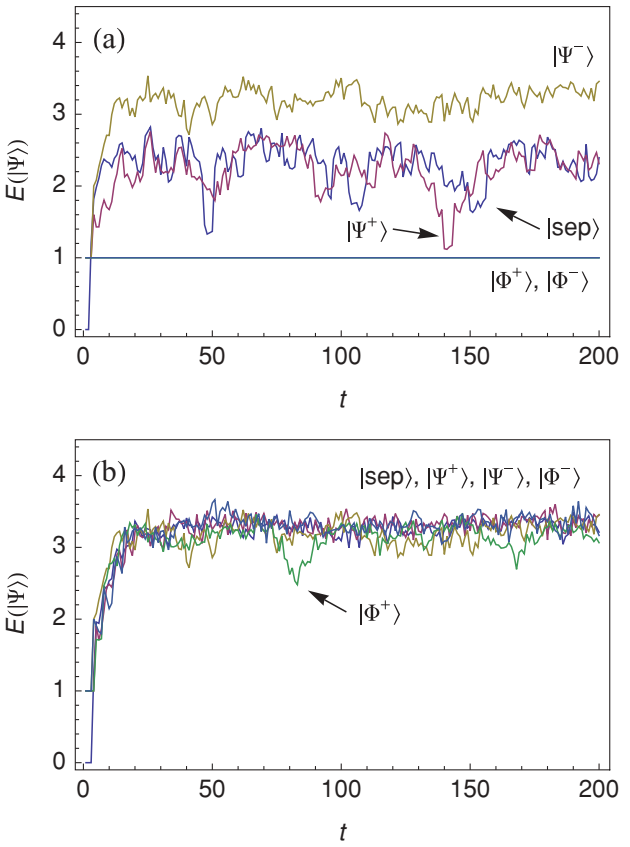

FIG. 6. (Color online) Time evolution of the entanglement between the two particles for (a) the $\mathbb{1}$-interacting and (b) the π-phase interacting quantum walk on the 16-cycle using the Hadamard coin, from initial states shown. $E_{\max} = 5$.

generates significant entanglement throughout the evolution of the walk.

In the $\mathbb{1}$-interacting quantum walk on the infinite line [Fig. 5(a)], the entanglement generated from initial states $|\text{sep}\rangle$ and $|\Psi^+\rangle$ rapidly approaches its asymptotic value, while that from the antisymmetric initial state $|\Psi^-\rangle$ appears to increase logarithmically with time. If we compare these results with the two-particle probability distributions shown in Figs. 3(a), 4(a), and 4(c), we see that both the $|\text{sep}\rangle$ and $|\Psi^+\rangle$ initial states result in two-particle distributions in which the particles are likely to be located at opposite ends of the line, whereas in the $|\Psi^-\rangle$ case, the two particles, even after 25 steps, are likely to be found at the same position. In effect, the $\mathbb{1}$ interaction results in rapid spatial separation of the two particles from initial states $|\text{sep}\rangle$ and $|\Psi^+\rangle$, preventing the generation of greater entanglement at later times. For the $|\Psi^-\rangle$ initial state, the entanglement continues to increase at later times because the interaction continues to act on doubly occupied states, which form a considerable portion of the distribution.

As discussed in Sec. III, the π-phase interaction generates two-particle probability distributions in which the two-particles have a reasonably large probability of being found at the same position for all initial states. By maintaining the two particles at the same position the π-phase interaction continues to generate entanglement between the particles for all initial states, even at later stages of the walk.

Greater entanglement introduced by the π-phase interaction is also observed on the 16-cycle (Fig. 6); however, rather than increasing logarithmically, the entanglement for all initial states rapidly increases to an asymptotic value of ≈ 3.2 ($\approx 0.65 E_{\max}$).

The entanglement between the two particles can also be calculated for two-particle quantum walks on graphs. In Sec. V, we study two-particle quantum walks on strongly regular graphs in the context of graph isomorphism testing. It is therefore interesting to see how the interactions introduced here entangle the two particles for quantum walks on strongly regular graphs.

Since the dimension of the single-particle coin Hilbert space $\mathcal{H}_C$ is equal to the degree of the graph, even if both particles start at the same position there are many possible initial states to consider. In addition, if the graph is not vertex- and edge-transitive then these initial states depend on the particular vertex and coin states chosen to be occupied in the initial state, since they are not all equivalent. We consider the following initial states,

$$|\xi\rangle = \sum_{i,j}^{d} |1,c_i;1,c_j\rangle, \tag{23}$$

$$|\zeta\rangle = |1,c_2;2,c_1\rangle + |2,c_1;1,c_2\rangle, \tag{24}$$

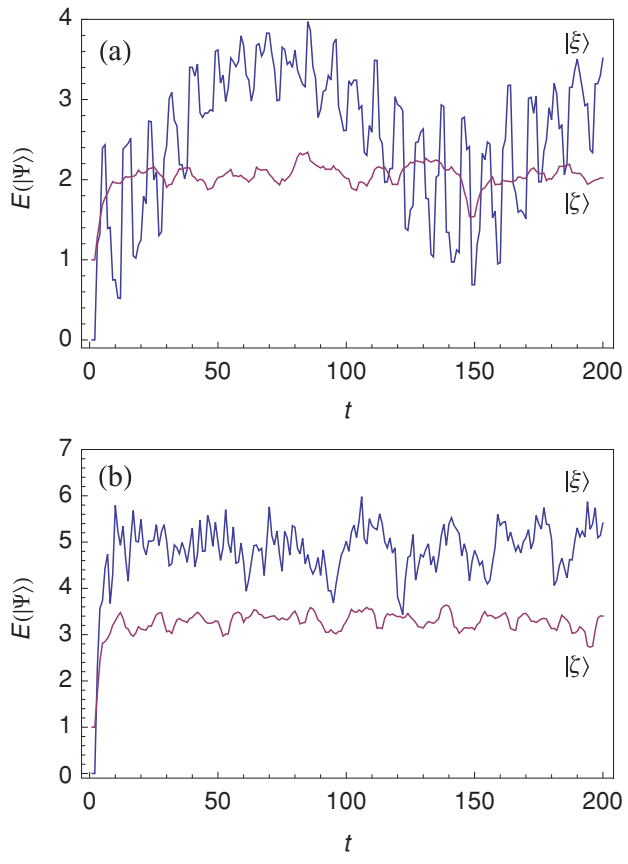

FIG. 7. (Color online) Time evolution of the entanglement between the two particles for (a) the $\mathbb{1}$-interacting and (b) the π-phase interacting quantum walk on a strongly regular graph with family parameters (16,6,2,2), from initial states shown.

where vertices 1 and 2 are chosen randomly on the graph. Note that $|\xi\rangle$ is separable [$E(|\xi\rangle) = 0$] but $|\zeta\rangle$ is entangled with $E(|\zeta\rangle) = 1$. As shown in Fig. 7, entanglement is generated by both the π-phase interaction and the $\mathbb{1}$ interaction for both of these initial states. Once again we see that the π-phase interaction generates greater entanglement between the particles than the $\mathbb{1}$ interaction.

V. GRAPH ISOMORPHISM TESTING

We now investigate the application of two-particle discrete-time quantum walks to the graph isomorphism problem.

Two graphs G and H are *isomorphic* if there exists a bijection $f : V(G) \to V(H)$ such that v_i and v_j are adjacent in G if and only if vertices $f(v_i)$ and $f(v_j)$ are adjacent in H. Such a mapping f is called an *isomorphism*. In other words, two graphs are isomorphic if the vertices can be relabeled so that the graphs are identical. The graph isomorphism problem (GI) is the computational problem of determining whether two graphs are isomorphic [21]. It is a problem that attracts considerable attention in computational complexity studies since it is one of very few problems in NP that is not known to be in P or to be NP complete. While there are many classes of graphs for which it is computationally easy to solve GI, the best known general algorithm has an upper bound of $O(e^{\sqrt{N \log N}})$ [21,22].

One class of graphs, for which there is no known polynomial-time GI algorithm, is the strongly regular graphs (SRGs). A SRG with parameters (N,d,λ,μ) is an undirected graph on N vertices in which each vertex has degree d, each pair of adjacent vertices have exactly λ common neighbors, and each pair of nonadjacent vertices have exactly μ common neighbors. SRGs are categorized into families based on their parameters (N,d,λ,μ) with each family possibly having many nonisomorphic members [23].

There have been several recent attempts to generate physically motivated GI algorithms [5,24–26]. Using discrete-time quantum walks, Douglas and Wang [24] developed a single-particle GI algorithm that successfully distinguished all pairs of graphs tested, including all SRGs with up to 64 vertices (over 40 000 graphs in total). In order to generate probability distributions which differ for nonisomorphic SRGs of the same family, it was necessary to perturb the quantum walks by applying different phase shifts to two different vertices of the graph at each time step.

Other studies by Shiau *et al.* [5] and Gamble *et al.* [6] have examined continuous-time quantum walks on SRGs and have found that the dynamics of (unperturbed) single-particle and *noninteracting* two-particle quantum walks are completely determined by the SRG family parameters (N,d,λ,μ). These walks cannot, therefore, be used to distinguish nonisomorphic SRGs from the same family. By introducing an interaction between the particles, these studies were able to successfully distinguish all nonisomorphic SRGs tested. While it was left as an open problem in [5] and [6] whether this algorithm solved GI in general, it has since been shown that there are pairs of nonisomorphic graphs for which this algorithm fails, even if extended to k-particle walks for arbitrary k [27]. The pairs of graphs for which this interacting two-particle algorithm has been proven to fail are not strongly regular graphs, so it remains

an open question whether interacting two-particle continuous-time quantum walks can distinguish arbitrary SRGs [27].

Given the demonstrated algorithmic differences between continuous- and discrete-time quantum walks [28], we find it interesting to consider whether two-particle quantum walks in discrete time can be used to distinguish SRGs. Continuous-time walks have no "coin" degrees of freedom so the Hilbert space on which the quantum walk takes place is spanned by N orthonormal vertex states. The state space of the k-particle continuous-time quantum walk therefore has dimension N^k. Conversely, the discrete-time quantum walk for a single particle on a d-regular graph takes place on a Hilbert space of dimension dN. So when this is extended to k particles, the dimension of the space grows to $(dN)^k$. It is interesting to consider whether these extra dimensions can be used to give discrete-time quantum walks greater graph-distinguishing power.

A. Description of the testing procedure

In order to distinguish two graphs, the two-particle probability distributions resulting from quantum walks on those graphs must differ whenever the graphs are nonisomorphic. To investigate the distinguishing power of two-particle quantum walks, we directly compare the two-particle probability distributions obtained on different graphs. This is achieved by applying the two-particle quantum walk operator U a fixed number of times to some initial state, and computing a certificate based on the two-particle probability distribution obtained. The certificates of each graph are then sorted and compared.

Not all initial states will permit differences in graph structure to be detected. For example, the equal superposition of all two-particle subnode states on a regular graph is an eigenvector of the two-particle quantum walk operator U in both the noninteracting and $\mathbb{1}$-interacting cases, so the probability distributions obtained from this initial state are trivial and cannot be used to distinguish graphs. An initial state must therefore have some asymmetry to produce nontrivial dynamics.

We also require that the GI certificate computed for a graph depend only on the geometric relationship between the vertices and not on a particular labeling. That is, the certificate must be identical for all possible permutations of the vertex set. In the context of computing a GI certificate, this means that if the walk is started at, say, two particular subnodes, then we need to cycle over all possible selections of those subnodes within the graph, to eliminate the dependence on labeling. With this in mind, we consider a state in which the particles are initially in a superposition of adjacent vertex states, with their coin states corresponding to the edge joining the two vertices,

$$|\beta^+\rangle = \frac{1}{\sqrt{2}}(|v_i,c_j\,;v_j,c_i\rangle + |v_j,c_i\,;v_i,c_j\rangle). \qquad (25)$$

These states will be referred to as *bosonic edge states*. Notice that each particle is delocalized across an edge rather than being in a single vertex state and also that the state is symmetric under particle exchange. The entanglement between the particles in this state is $E = 1$. On a d-regular graph with N vertices, there are only $Nd/2$ distinct states of this form. The number of initial states which must be cycled over therefore scales as $O(dN)$, with $d < N$.

The following procedure is used to generate a graph certificate based on the two-particle probability distribution.

(1) Starting in an initial bosonic edge state $|\beta^+\rangle$, perform $2N$ steps of the two-particle quantum walk on a graph, storing the values $\sum_{t=1}^{2N} P(i,j,t)$ for all $i,j \in [1,N]$. This generates a list of length N^2. $2N$ steps are performed to ensure that the geometry of the graph is adequately sampled by the particles.

(2) Repeat step 1 for all $Nd/2$ possible initial states, concatenating values obtained for each initial state into a total list of length $N^3d/2$.

(3) Construct the certificate of the graph, consisting of a sorted list containing each distinct value obtained in steps 1 and 2 along with the number of times the value occurred.

By cycling over all possible initial states, the dependence on the labeling of the vertices is eliminated, so that two isomorphic graphs necessarily produce the same certificate. This fact was also verified numerically by comparing the certificates produced by permutations of a single SRG.

Computationally, the most complex procedure in the two-particle quantum walk is performing the N^2 coin operations at each step. On a d-regular graph the coin is a $d^2 \times d^2$ matrix so the $2N$-step quantum walk has time complexity $O(N^3d^4)$. Cycling over all $Nd/2$ initial states gives a classical upper bound for the time complexity of the above computation of $O(N^4d^5)$.

B. GI certificates for noninteracting particles

The first four rows in the GI certificates of the two nonisomorphic SRGs in the (16,6,2,2) family (Fig. 8) are shown in Table I. It can be seen that these graphs are easily distinguished using noninteracting two-particle quantum walks. It is worth recalling that the corresponding continuous-time algorithm would fail in this case [6], since the dynamics of noninteracting two-particle continuous-time quantum walks depend entirely on the SRG family parameters (N,d,λ,μ). This finding immediately highlights a difference in the algorithmic capability of the two formulations of quantum walks.

The SRGs tested are shown in Table II. It was found that two noninteracting particles successfully distinguished all members of most of the families tested. There are, however, nonisomorphic graphs with 36 and 40 vertices which produce the same noninteracting two-particle GI certificates using the above method. Two such graphs in the (40,12,2,4) family are nonisomorphic 3-isoregular graphs, which are an extension of strongly regular graphs that have the additional requirement that the set of neighbors and nonneighbors of each vertex are also SRGs [29]. Due to the additional symmetry, we expect

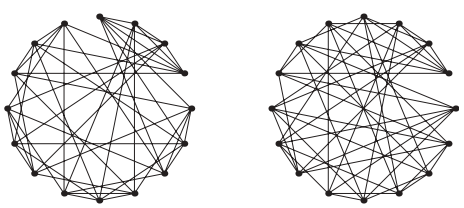

FIG. 8. The two nonisomorphic SRGs with family parameters (16,6,2,2).

TABLE I. The first four entries in the certificates computed for noninteracting two-particle quantum walks on the two nonisomorphic strongly regular graphs with family parameters (16,6,2,2) (shown in Fig. 8). "No." represents the number of occurrences of the $\sum_{t=1}^{N} P(i,j,t)$ values.

Graph 1		Graph 2	
$\sum_{t=1}^{N} P(i,j,t)$	No.	$\sum_{t=1}^{N} P(i,j,t)$	No.
0.0080650955	1728	0.0064520764	960
0.0098066692	3456	0.0080650955	768
0.0176278617	864	0.0098066692	768
0.0180697993	1152	0.0109051753	1152
⋮	⋮	⋮	⋮

that these graphs are very difficult to distinguish. We also analyzed the other sets of graphs in this family for which the algorithm failed using the graph analysis package NAUTY [30]. The automorphism groups for these graphs were found to have various sizes and the orbit structures are distinct within the sets of non-distinguished graphs. Further graph-theoretic analysis is required to determine the graph-structural basis for the failure of the method in these cases.

C. GI certificates for $\mathbb{1}$-interacting particles

Using two-particle quantum walks with $\mathbb{1}$ interaction, GI certificates were computed for the graphs listed in Table II. This resulted in unique GI certificates for all nonisomorphic SRGs tested, demonstrating that explicit interaction significantly increases the graph-distinguishing power of the two-particle quantum walk.

In order to determine whether entanglement between the two particles in the initial state is an important part of this algorithm, we also considered a similar initial state which is again delocalized over two vertices but which is now separable in the two particles,

$$|\beta^{\text{sep}}\rangle = \tfrac{1}{2}(|v_i,c_j\,;v_i,c_j\rangle + |v_i,c_j\,;v_j,c_i\rangle + |v_j,c_i\,;v_i,c_j\rangle + |v_j,c_i\,;v_j,c_i\rangle). \quad (26)$$

The GI certificates for the (36,14,4,6) and (40,12,2,4) families were computed using the method outlined above, this time using the separable initial states $|\beta^{\text{sep}}\rangle$. While these certificates were different from the entangled case, the same sets of graphs were successfully distinguished. Antisymmetric "fermionic" edge states also produced identical results, suggesting that the distinguishing power of the two-particle algorithm comes from delocalization of the initial state rather than initial entanglement between the two particles.

TABLE II. Sets of nonisomorphic strongly regular graphs tested by computing the noninteracting and interacting two-particle quantum walk GI certificates. The "Yes" indicates that all nonisomorphic family members produced unique GI certificates, while "No" indicates that some graphs in the family produced identical certificates. The "-" indicates that the family was not tested.

		All Graphs Distinguished?	
(N,d,λ,μ)	Group Size	Noninteracting	Interacting
(16,6,2,2)	2	Yes	Yes
(25,12,5,6)	15	Yes	Yes
(26,10,3,4)	10	Yes	Yes
(28,12,6,4)	4	Yes	Yes
(29,14,6,7)	41	Yes	Yes
(35,16,6,8)	3854	-	Yes
(36,14,4,6)	180	No	Yes
(40,12,2,4)	28	No	Yes

D. This procedure cannot distinguish arbitrary graphs

Quantum-walk-based GI algorithms are, in some respects, similar to a classical GI algorithm known as Weisfeiler-Leman (W-L) vertex refinement, which typically distinguishes pairs of nonisomorphic graphs in polynomial time. In fact, recent studies have suggested a direct correspondence between the two methods [31]. It has been shown by Cai, Fürer, and Immerman, however, that for certain graphs, there exist two related graphs, which cannot be distinguished by the W-L method in polynomial time [32], thus proving that the W-L method is not a polynomial-time algorithm for GI.

To test whether or not the interacting two-particle quantum-walk procedure described above can distinguish pairs of these graphs, we constructed a pair of Cai-Fürer-Immerman graphs with 80 vertices and computed their GI certificates using the above procedure with $\mathbb{1}$ interaction. Both graphs in the nonisomorphic pair produced the same certificate, demonstrating that the procedure, in its current form, cannot distinguish arbitrary graphs. Nonetheless, this technique provides an interesting tool for computer scientists interested in GI. In particular, recent work by Douglas [31] has shown that the Weisfeiler-Leman method can however be extended to distinguish all known counterexamples. It is therefore possible that a quantum-walk-based graph isomorphism testing procedure could also be extended in a similar fashion.

VI. CONCLUSION

We have introduced two related schemes that allow spatial interactions between particles in two-particle discrete-time quantum walks. While maintaining purely unitary dynamics, these interactions have been shown to generate single-particle probability distributions that depend on the correlations and the relative phases between the initial coin states of the two particles. It was also shown that these interactions generate spatial correlations and entanglement between the particles undergoing the quantum walk. In particular, the π-phase interaction was shown to generate two-particle probability distributions with specific spatial correlations from all localized initial states studied.

These interaction schemes can also be applied to quantum walks on arbitrary undirected graphs. In Sec. V, we discussed

an application of discrete-time two-particle quantum walks to the graph isomorphism problem. The graph-distinguishing power of the walks was examined by computing and comparing GI certificates based on the two-particle probability distributions. In contrast to continuous-time quantum walks, it was shown that two noninteracting particles can distinguish some (but not all) nonisomorphic SRGs with the same family parameters. In addition, the GI certificates produced in the interacting quantum walk successfully distinguished all nonisomorphic graphs tested, which is equivalent to the results obtained for the continuous-time quantum walk with two interacting bosons [5,6]. While the continuous-time interaction was implemented by incorporating an energy cost in the Hamiltonian for multiply occupied quantum states (or by using hard-core bosons), it is interesting to see that the simple spatial interaction introduced here leads to similar graph-distinguishing power.

Algorithmic applications of the diverse single- and two-particle probability distributions obtained by performing quantum walks with interacting and entangled particles will be an interesting subject for further study.

ACKNOWLEDGMENTS

The authors would like to thank Brendan Douglas and Shaoming Fei for critical comments and suggestions. SDB thanks the John and Patricia Farrant foundation for financial support. The authors also acknowledge iVEC–'The hub of advanced computing in Western Australia,' for technical support and use of their SGI Altix supercomputer.

[1] J. Kempe, Contemp. Phys. **44**, 307 (2003).
[2] M. Santha, in *Theory and Applications of Models of Computation*, Lecture Notes in Computer Science, Vol. 4978, edited by M. Agrawal, D. Du, Z. Duan, and A. Li (Springer, Berlin/Heidelberg, 2008), pp. 31–46.
[3] Y. Omar, N. Paunković, L. Sheridan, and S. Bose, Phys. Rev. A **74**, 042304 (2006).
[4] P. K. Pathak and G. S. Agarwal, Phys. Rev. A **75**, 032351 (2007).
[5] S.-Y. Shiau, R. Joynt, and S. Coppersmith, Quantum Inf. Comput. **5**, 492 (2005).
[6] J. K. Gamble, M. Friesen, D. Zhou, R. Joynt, and S. N. Coppersmith, Phys. Rev. A **81**, 052313 (2010).
[7] F. Zähringer, G. Kirchmair, R. Gerritsma, E. Solano, R. Blatt, and C. F. Roos, Phys. Rev. Lett. **104**, 100503 (2010).
[8] A. Peruzzo *et al.*, Science **329**, 1500 (2010).
[9] M. Štefanák, T. Kiss, I. Jex, and B. Mohring, J. Phys. A **39**, 14965 (2006).
[10] P. P. Rohde, A. Schreiber, M. Štefaňák, I. Jex, and C. Silberhorn, New J. Phys. **13**, 013001 (2011).
[11] S. E. Venegas-Andraca and S. Bose, e-print arXiv:0901.3946v1.
[12] I. Carneiro, M. Loo, X. Xu, M. Girerd, V. Kendon, and P. L. Knight, New J. Phys. **7**, 156 (2005).
[13] D. Aharonov, A. Ambainis, J. Kempe, and U. Vazirani, in *STOC '01: Proceedings of the Thirty-third Annual ACM Symposium on Theory of Computing* (ACM, New York, 2001), pp. 50–59.
[14] N. Shenvi, J. Kempe, and K. B. Whaley, Phys. Rev. A **67**, 052307 (2003).
[15] A. Ambainis, E. Bach, A. Nayak, A. Vishwanath, and J. Watrous, in *STOC '01: Proceedings of the Thirty-third Annual ACM Symposium on Theory of Computing* (ACM, New York, 2001), pp. 37–49.
[16] O. Maloyer and V. Kendon, New J. Phys. **9**, 87 (2007).
[17] C. Liu and N. Petulante, Math. Structures Comput. Sci. **20**, 1099 (2010).
[18] M. Annabestani, M. R. Abolhasani, and G. Abal, J. Phys. A **43**, 075301 (2010).
[19] S. K. Goyal and C. M. Chandrashekar, J. Phys. A **43**, 235303 (2010).
[20] F. Mintert, A. R. Carvalho, M. Kus, and A. Buchleitner, Phys. Rep. **415**, 207 (2005).
[21] J. Köbler, in *Logical Approaches to Computational Barriers*, Lecture Notes in Computer Science, Vol. 3988, edited by A. Beckmann, U. Berger, B. Löwe, and J. Tucker (Springer, Berlin/Heidelberg, 2006), pp. 241–256.
[22] L. Babai and E. M. Luks, in *STOC '83: Proceedings of the Fifteenth Annual ACM Symposium on Theory of Computing* (ACM, New York, 1983), pp. 171–183.
[23] C. Godsil and G. Royle, *Algebraic Graph Theory* (Springer, New York, 2001).
[24] B. L. Douglas and J. B. Wang, J. Phys. A **41**, 075303 (2008).
[25] D. Emms, R. C. Wilson, and E. R. Hancock, in *7th IAPR-TC15 Workshop on Graph-based Representations (GbR 2007)* [Image and Vision Computing **27**, 934 (2009)].
[26] D. Emms, R. C. Wilson, and E. R. Hancock, Pattern Recognition **42**, 985 (2009).
[27] J. Smith, e-print arXiv:1004.0206v1.
[28] A. Ambainis, J. Kempe, and A. Rivosh, in *SODA '05: Proceedings of the Sixteenth Annual ACM-SIAM Symposium on Discrete Algorithms* (Society for Industrial and Applied Mathematics, Philadelphia, 2005), pp. 1099–1108.
[29] S. Reichard, J. Comb. Theory, Ser. A **90**, 304 (2000).
[30] B. D. McKay, NAUTY User's Guide (Version 2.4), Australian National University, Canberra, Australia, 2009.
[31] B. L. Douglas (private communication); e-print arXiv:1101.5211v1.
[32] J.-Y. Cai, M. Fürer, and N. Immerman, Combinatorica **12**, 389 (1992).